frontiers | Frontiers in Marine Science

TYPE Original Research
PUBLISHED 09 December 2024
DOI 10.3389/fmars.2024.1458758

OPEN ACCESS

EDITED BY
Changsheng Chen,
University of Massachusetts Dartmouth, United States

REVIEWED BY
Zhigang Lai,
Sun Yat-sen University, China
Jianzhong Ge,
East China Normal University, China

*CORRESPONDENCE
Elias Pinilla
elias.pinilla@umaine.edu

RECEIVED 03 July 2024
ACCEPTED 14 November 2024
PUBLISHED 09 December 2024

CITATION
Pinilla E, Ross L and Pérez-Santos I (2024) Exchange flow in a highly stratified fjord in drought conditions.
Front. Mar. Sci. 11:1458758.
doi: 10.3389/fmars.2024.1458758

Exchange flow in a highly stratified fjord in drought conditions

Elias Pinilla[1,2]*, Lauren Ross[1] and Iván Pérez-Santos[3,4,5]

[1]Department of Civil and Environmental Engineering, University of Maine, Orono, ME, United States, [2]Instituto de Fomento Pesquero, CTPA-Putemún, Castro, Chiloé, Chile, [3]Centro i-mar de la Universidad de los Lagos, Puerto Montt, Chile, [4]Center for Oceanographic Research COPAS COASTAL, Universidad de Concepción, Concepción, Chile, [5]Centro de Investigaciones en Ecosistemas de la Patagonia (CIEP), Coyhaique, Chile

Fjords are known for their biodiversity and abundant aquaculture resources. However, climate and anthropogenic pressures are altering fjord biological, physical, and chemical processes that will undoubtedly change the ecosystem as a whole. To investigate the impact of climate change on fjord functioning, this study examines the impacts of drought conditions on the physical dynamics and salinity variations in a fjord known for its bolstering aquaculture industry in Northern Chilean Patagonia, the Reloncaví Fjord (41.5° S). Using a high-resolution hydrodynamic model and the Total Exchange Flow (TEF) framework, we analyzed the impacts of river discharge, tides, and wind during a dry year (2016) and a typical year (2018). In 2016, reduced freshwater input decreased exchange flow and increased salinity compared to 2018. In 2018, river discharge dominated TEF variability (74%), while tides and wind contributed 17% and 9%, respectively. In summer 2016, tidal and wind influences rose to 21% and 16%, highlighting their role under low freshwater conditions. Increased wind facilitated destratification, mixing high-salinity subsurface waters with fresh surface layers, affecting ecosystem dynamics. From these results we developed a method to predict long-term stratification variability (1980–2021), identifying critical ecological shifts. Logistic regression models showed significant links between stratification levels and harmful algal blooms (HABs) of *Pseudchatonella* spp. and *Alexandrium catenella*. Lower stratification was linked to higher *Pseudchatonella* spp. HABs in summer, while higher stratification correlated with *Alexandrium catenella* blooms in spring, tied to increased river discharge. These results suggest that severe HAB events in Northern Patagonia may become more frequent with climate change, underscoring the need to consider local environmental dynamics and stratification in HAB studies.

KEYWORDS

Total Exchange Flow (TEF), fjord, estuary, stratification, drought, tides, harmful algal blooms (HABs), climate change

1 Introduction

Fjords are characteristically long, narrow, and deep inlets with steep sides and one or more submarine sills (Inall and Gillibrand, 2010). These systems are often strongly stratified due to significant freshwater input which leads to a thin surface layer of freshwater outflow over a thick bottom layer of saline inflow, creating a buoyancy force that can inhibit vertical shear-driven mixing (Geyer and Ralston, 2011; Valle-Levinson, 2010). Fjords are abundant and diverse in high latitudes, and are prevalent in Chilean Patagonia, a region that spans the southern tip of South America from ~41° to 55.9°S. Patagonian fjords host a rich marine biodiversity, including endemic species and endangered marine mammals, such as whales and dolphins (Hucke-Gaete et al., 2004; Buchan et al., 2010; Viddi et al., 2010; Bedriñana-Romano et al., 2023). In addition, fjords store 11 to 12% of the total organic carbon in the global ocean yet cover only ~0.1% of the ocean surface area (Smith et al., 2015; Cui et al., 2022), highlighting their importance in climate regulation. Fjords in Chilean Patagonia also support a thriving finfish aquaculture industry, which has made Chile the world's second largest producer of farmed salmon, after Norway (Food and Agriculture Organization of the United Nations (FAO), 2022).

Climate variability in Chilean Patagonia has been found to impact the frequency and severity of extreme events (Díaz et al., 2023; Mardones et al., 2021), altering the hydrological balance of watersheds and the freshwater input to fjords (Aguayo et al., 2019). For example, Patagonia faced an extreme drought in the summer and fall of 2016, causing reduced river discharge and environmental disturbances like major forest fires and harmful algal blooms (HABs) (Garreaud, 2018; León-Muñoz et al., 2018; Mardones et al., 2021). These changes were linked to a strong El Niño and the influence of the Southern Annular Mode (SAM) compounded with climate and anthropogenic change (Garreaud, 2018; León-Muñoz et al., 2018; Mardones et al., 2021). Future projections suggest northern Patagonia will experience more frequent extreme droughts, like the one in 2016, due to the worsening effects of climate change, which will become especially prominent during El Niño events (Garreaud, 2018). Aguayo et al. (2019) studied the impact of climate change on the Puelo River's hydrology, a crucial freshwater source in Chile's Northern Patagonia. Under the 'Representative Concentration Pathway' (RCP) 8.5 scenario they projected by 2030-2060 there will be a 10% annual freshwater decrease to the Reloncaví Fjord, which houses the majority of finfish aquaculture and is the main producer of mussel seed in the region. They also anticipate that extreme hydroclimatic events, like the significant 2016 drought, will double in frequency by 2030-2060 (Aguayo et al., 2019).

Considering the impact that climate and anthropogenic change is expected to have on the hydrological and ecological dynamics of fjord regions, it becomes evident that baseline fjord circulation and exchange patterns will also likely shift. Estuarine circulation is commonly defined as a two-layer circulation with a seaward flowing surface layer and a landward flowing subsurface layer (Shan et al., 2019). However, Valle-Levinson et al. (2014) showed that the circulation in fjords can evolve into varied vertical structures influenced by additional forces such as wind, remote factors such as density gradients, and tidal dynamics. Wind forcing, as detailed in studies by Giddings and MacCready (2017); Lange et al. (2020); Wan et al. (2022), and Soto-Riquelme et al. (2023), can significantly reshape the traditional two-layer model, potentially creating a more complex flow pattern. Soto-Riquelme et al. (2023) found that in Patagonian fjords, wind dynamics play a key role, with up-channel winds in winter disrupting density driven circulation and causing a three-layer vertical structure with surface inward flow. During spring and summer, downchannel winds enhanced two-layer estuarine circulation.

Remote forcing can also play a crucial role in the hydrodynamics of fjords. Density gradients in adjacent waters can lead to baroclinic pumping, as described by Stigebrandt (2012), which impacts the circulation within the fjord by imposing horizontal pressure gradients that alter water movement through the fjord's mouth (Stigebrandt, 1990; Engqvist and Omstedt, 1992; Aure et al., 1996). According to Arneborg et al. (2004), in most of the fjords and inlets along the Swedish and Norwegian coasts, and the Baltic Sea, density fluctuations on the coast are the most important forcing mechanisms for water exchange. However, tidal forces add another dimension of complexity to fjord circulation. Theoretical analyses by Ianniello (1977) and later by Winant (2008) suggest that in deeper fjords, tidal forces can induce a three-layer residual flow. Valle-Levinson et al. (2014) offered observational support for this theory in Patagonian fjords, that tidal action can create this additional layer, emphasizing the need to consider a broader range of dynamic processes when analyzing subtidal circulation in fjords. However, these studies focused on understanding the strength and structure of residual flows without considering the effects of climate change. They also used Eulerian averages to quantify the subtidal circulation, which leaves out tidal pumping effects that could be important when quantifying the volume of exchange over long time scales.

The Total Exchange Flow (TEF) framework, as proposed by MacCready (2011), offers a robust methodology for quantifying the time-averaged net transport of volume and mass between the ocean and estuaries, segmented by salinity classes. This approach is particularly relevant for fjords in Northern Patagonia, where tidal amplitudes due to resonance phenomena are notable (Cáceres et al., 2003; Aiken, 2008), making the tidal influence on exchange flow potentially significant. The overall goal of this study is to determine how extreme drought conditions affect the physical functioning of stratified fjords. To reach this goal two specific research questions will be answered: 1) How does TEF vary in a stratified fjord throughout a drought year (2016) with low freshwater inflow and a year with typical freshwater inflow (2018), and 2) What is the relative importance of wind and tidal forcing on exchange flow between these two years? To answer these questions, we use numerical simulations of Reloncaví Fjord in Northern Patagonia to quantify the TEF during the drought and typical years. Reloncaví Fjord is known for its prolific salmon farming industry, which is extensive, yet sensitive to environmental changes. Notably, a harmful algal bloom (HAB) during the 2016 drought caused significant economic and ecological damage, with losses surpassing $800 million USD from the mortality of 40,000 tons of

salmon, creating a social and sanitary crisis (León-Muñoz et al., 2018). The drought condition that Reloncaví Fjord faced in 2016 is the motivation for choosing it as a case study area. The work presented here underscores the urgent need to understand the intrinsic nature of fjord systems, especially those transitioning due to climate change, and the broader potential ecological implications of these shifts.

2 Study area

The Reloncaví Fjord is approximately 55 km long and on average 2.3 km wide with depths varying greatly from the head to the mouth of the fjord (Figure 1). The fjord is shallow upstream of the Cochamó River to the head of the fjord, where the Petrohué River is located, and in this region has an average depth of 50 m. The fjord is deepest, with an average depth of 400 m, close to the mouth. To the north and south of the Puelo River at the mid-reaches of the fjord, the average depths are 270 and 220 m, respectively (Castillo et al., 2012) (Figure 1). The fjord is surrounded by mountainous terrain on all sides and connects to the adjacent Reloncaví Sound.

Located in a temperate region, the Reloncaví Fjord experiences a snow-rain hydrological regime. These mixed regime patterns govern the river discharge in the area, with rivers reaching peak flows during winter (by rain) and spring (by snow melting) (Niemeyer and Cereceda, 1984). Among the rivers feeding into the fjord, the Puelo River is not only the largest in the area, but is also one of the largest in Patagonia, with an annual average discharge of approximately 650 m^3s^{-1} (Niemeyer and Cereceda, 1984). The main peak is in winter due to precipitation (May–July average: 771–866 m^3s^{-1}) with a secondary, snowmelt peak in late spring (November–December average: 712–761 m^3s^{-1}) (Lara et al., 2005). This river's average discharge is roughly double that of the Petrohué River, which itself has an average annual discharge of 280 m^3s^{-1} (León, 2005). The Petrohué River reaches its peak flow during winter, with maximum discharges of around 450 m^3s^{-1} (Castillo et al., 2012). In addition to these primary rivers, freshwater input to the Reloncaví Fjord is supplemented by several smaller sources. The Cochamo River, for example, contributes an average annual discharge of 20 m^3s^{-1}, while the nearby Canutillar hydroelectric plant adds around 75.5 m^3s^{-1} to the system's freshwater inflow (Castillo et al., 2012).

The Reloncaví Fjord is typically strongly stratified throughout the year with a thin surface layer of brackish water with mean salinities between 10.4 ± 1.4 g kg^{-1} in spring and 13.2 ± 2.5 g kg^{-1} in autumn (Castillo et al., 2012). Beneath the surface layer, changes in salinity are considerably less pronounced. For example, at 20 m depth, the salinity was found to be 32.2 g kg^{-1}, increasing to 32.8 g kg^{-1} below 250 m depth close to the mouth in the study by Castillo et al. (2012). The winds are mainly down-fjord during winter (east to west), reinforcing the outflow of the freshwater upper layer, while the winds blow predominantly up-fjord during spring and summer (west to east) (Castillo et al., 2012). Inside the fjord (near the Puelo River), the maximum tidal amplitude is 6 m and tidal current velocities are approximately 0.1 m s^{-1} (Valle-Levinson et al., 2007).

Castillo et al. (2012) analyzed current velocity data collected from July to November 2008 during a typical hydrological year. They found a three-layer vertical pattern in the residual along-fjord circulation within Reloncaví Fjord with a thin (<5 m) outflow in the upper layer, a thick intermediate inflow layer (>5 m and <100 m) and a weak deep (>100 m) outflow layer (Valle-Levinson et al., 2007; Castillo et al., 2012). Castillo et al. (2012) revealed that along-channel advective terms were the most relevant in producing this three-layer vertical residual flow structure. However, near the Puelo River, where the fjord curves sharply and there is a strong baroclinic influence from river input, both advective and frictional forces were relevant.

3 Methodology

3.1 Hydro-meteorological data and analysis

To understand the general conditions and trends of the hydrological and atmospheric variables that influence the Reloncaví Fjord region, we analyzed meteorological data from 1980 to 2020. The atmospheric data were obtained from the CR2MET dataset (Boisier, 2023), (http://www.cr2.cl/datos-productos-grillados/) and ERA5. The ERA5 is the latest climate reanalysis produced by the European Centre for Medium-Range Weather Forecasts (ECMWF) under the Copernicus Climate Change Service (https://climate.copernicus.eu). The ERA5 dataset extracted for this study includes mean sea level (MSL) pressure (atmospheric pressure) and CR2MET provides precipitation data, both of which are from a grid point close to the Puelo River (Figure 1B). The hydrological data include discharge values from the Puelo River, which are modeled by the FLOW-IFOP hydrological system (Reche et al., 2021). This model utilizes precipitation and temperature time series data from the CR2MET gridded product to simulate runoff and calculate daily discharge time series for the period from 1980-2021.

To investigate long-term trends of these parameters, averages of MSL pressure, precipitation, and river discharge were calculated over the austral summer (January to March) from 1980 to 2020, followed by trend line estimation. This specific seasonal window was chosen for two key reasons: first, it coincides with the months of historically lowest river discharge (Niemeyer and Cereceda, 1984). Second, this seasonal window aligns with the time of historical biological activity in the fjord, in particular algal blooms (Mardones, 2020). The combination of low river discharge and high biological activity can interact and influence the system's dynamics, making this period particularly interesting for studying ecosystem dynamics. We calculated linear trends for each parameter (MSL pressure, precipitation, and river discharge) using a least-squares regression model. Uncertainty was assessed by calculating the standard error of the estimated slope. The statistical significance of the trends were evaluated using the p-value associated with the slope estimate. These analyses provide insights into how each parameter has changed over the study period and allow us to assess whether these changes are significant.

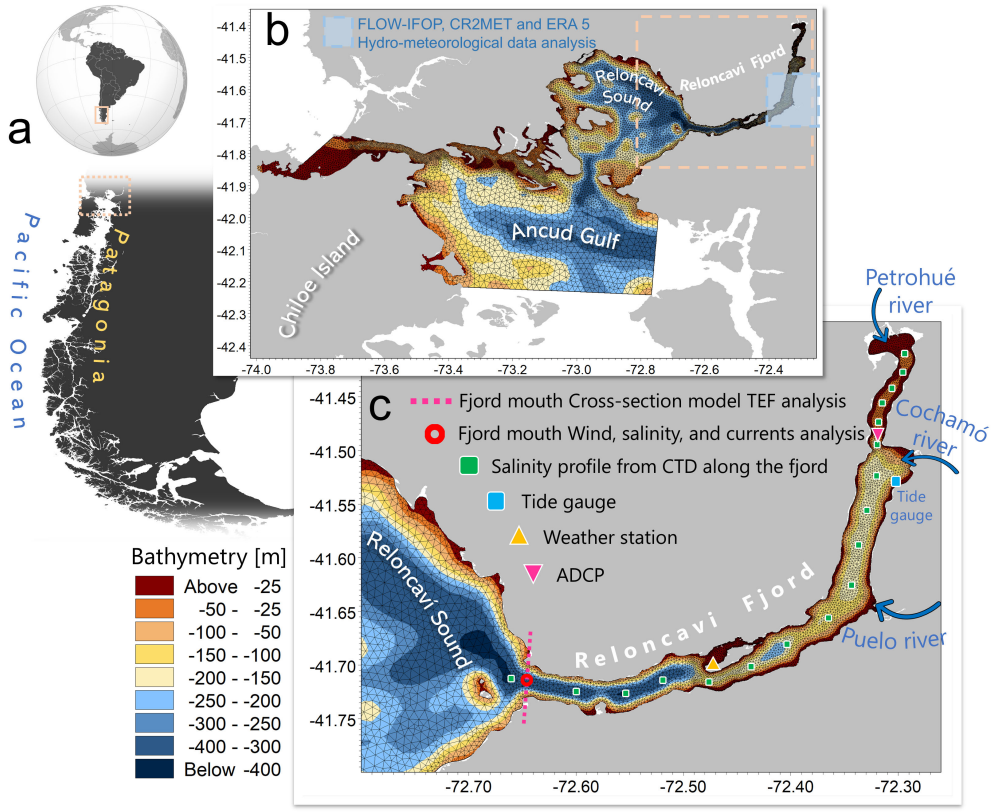

FIGURE 1
Study area and model domain. **(A)** Global map showing South America with a focus on Patagonia; the study area is highlighted within a box. **(B)** MIKE 3 FM hydrodynamic model domain with an unstructured mesh, centered on Northern Patagonia. The blue box marks the region used for hydro-meteorological data extraction. **(C)** Detailed view of the Reloncaví Fjord. The pink dashed line represents the cross-section at the fjord's mouth used for Total Exchange Flow (TEF) analysis. The red square indicates a data extraction point for salinity, current profiles, and surface wind data. Green squares show CTD stations used for model validation. The yellow triangle marks the location of a weather station, and the pink triangle marks the ADCP location, both used for model validation. The cyan square represents the position of the tide gauge near the fjord's head, also used for model validation. Major rivers are labeled, and the color bar illustrates the bathymetry.

3.2 Numerical models setup and simulations

A three-dimensional numerical model developed in MIKE 3 FM (Danish Hydraulic Institute (DHI), 2019) has been configured to simulate the hydrodynamics in the Reloncaví Fjord and the surrounding region. The model solves continuity, momentum, temperature, and salinity transport equations using the finite volume method (Danish Hydraulic Institute (DHI), 2019). In this study, the high-resolution model domain includes a large section of northern Patagonia including the Ancud Gulf, the inlet passage connecting the Ancud Gulf to the Pacific Ocean, Reloncaví Sound, and Reloncavi Fjord (Figure 1).

The model configuration is hydrostatic, with vertical discretization via hybrid coordinates that are sigma coordinates at the surface and z-level coordinates in the bottom layers. In total, there are 60 vertical layers, which were needed to accurately depict the near-surface stratification. In fact, the highest resolution of sigma coordinates, approximately 1 m vertical spacing, is in the upper water column. Horizontal eddy viscosity was characterized using the Smagorinsky formula (Smagorinsky, 1963), while the vertical eddy viscosity was incorporated through the κ–ϵ turbulence scheme. This scheme solves the transport equations for both turbulent kinetic energy (κ) and the turbulent dissipation rate (ϵ) (Launder and Spalding, 1974; Rodi, 1984). Bathymetry was based on SHOA (Servicio Hidrográfico y Oceanográfico de la Armada) nautical chart soundings, and a digital elevation model was constructed using the natural neighbor method (Sibson, 1981). The domain was discretized using an unstructured grid of triangular elements of different sizes. The highest resolution is in the narrow and shallow coastal areas, with an average element size of 50 m, whereas the spatial resolution near the boundary is approximately 1000 m.

The modeling period for this study extends from winter 2015 through 2018. For the purposes of this investigation, data from the years 2016 and 2018 were exclusively examined as representative 'dry' and 'typical' years, respectively. Boundary conditions for the study, such as temperature, salinity, current velocities, and sea level, were obtained from the regional hydrodynamic model 'D1-Chiloeé' (Pinilla et al., 2020), which has been extensively utilized in other studies (Mardones et al., 2021; Pérez-Santos et al., 2021; Landaeta et al., 2023; Linford et al., 2023). Additionally, 'D1-Chiloé' is freely

accessible on the CHONOS online platform at http://chonos.ifop.cl, promoting transparency and facilitating future research endeavors (Reche et al., 2021).

Freshwater inflows at the upstream model boundaries were derived from the FLOW-IFOP hydrological model. This model incorporates data from major rivers, specifically the Petrohué, Cochamó, and Puelo rivers, as illustrated in Figure 1, along with several other sources of considerably lesser magnitude. Based on FLOW-IFOP estimates, the average annual (1980-2021) freshwater discharge entering the Reloncaví Fjord was approximately 970 $m^3 s^{-1}$, with nearly 2/3 of this contribution from the Puelo River. The performance of the FLOW-IFOP model at the gauged river stations of the Chilean Water Authority is accessible on the Chonos Information System online platform (http://chonos.ifop.cl/flow/) (Reche et al., 2021).

Atmospheric drivers, including wind stress and heat fluxes across the sea surface, were incorporated into the model using spatially and temporally variable fields derived from the WRF-IFOP atmospheric model (Reche et al., 2021). The WRF model (Skamarock et al., 2008) has a spatial resolution of 3 km, offering a finer resolution than global models, yet it remains relatively coarse for capturing intricate topographical features and local wind details.

The different models were extensively validated in their ability to reproduce wind, river discharge, salinity, and current velocity data. Detailed validation results, including statistical comparisons with observational data, are provided in the Supplementary Material accompanying this manuscript.

To achieve the goals of this study, which include assessing the effects of river inflow, wind stress, and tides on exchange flow dynamics within Reloncavi Fjord, a series of process-oriented simulations were performed. The first, our base model denoted 'RTW-1', integrates all forcing components—rivers, tides, and wind. Subsequently, to isolate the impact of wind stress, a 'No-Wind' scenario, 'RT-2', was run using the same base configuration but omitting wind influence. Finally, a third model, 'R-3', incorporates only the riverine input. The 'R-3' model, while primarily considering river input, also accounts for external density changes from the 'D1-Chiloe' regional model's boundary conditions. This approach allows us to capture the estuarine variability driven not just by rivers but also by external density variations. Comparing the results from 'RTW-1' with those from 'RT-2' and 'R-3' allows for a detailed assessment of the contributions from each force separately, thereby enhancing our understanding of their individual roles in shaping the exchange flow. In addition, to isolate the contributions of tides, wind and river to the TEF, we will subtract the values of TEF outflow, Q_{out}, from one model run with another. For example, to isolate the contribution of tides to the TEF outflow, we will subtract Q_{out} from R-3 from Q_{out} from RT-2. It should be noted that when referring to 'tides' within our simulations, it is essential to clarify that we are focusing on the subtidal components of tidal dynamics. This means that while diurnal and semidiurnal tidal forces are included in our models, we specifically examine the effects beyond these tidal signals, mainly over fortnightly tidal cycles.

3.3 Total Exchange Flow (TEF)

The TEF analysis framework (MacCready, 2011) quantifies the transport of volume and salinity both into and out of the estuary in salinity space and employs isohaline coordinates to separate the inflow and outflow into salinity classes. TEF captures both tidal and subtidal dynamics to perfectly satisfy the Knudsen relations (Burchard et al., 2018). Following MacCready (2011), the tidally averaged (denoted by $\langle\rangle$) transport $Q(S)$ through the cross-sectional area $A(s > S)$, which has a salinity s above a specific value S is defined as:

$$Q(S) = \left\langle \int_{A(s>S)} u \, dA \right\rangle, \tag{1}$$

where u is the incoming velocity normal to $A(s > S)$. The exchange flow volume transport with respect to salinity class, $q(S)$, is then obtained by differentiating $Q(S)$ with respect to S,

$$q(S) = -\frac{\partial Q(S)}{\partial S}. \tag{2}$$

The negative sign in front of $\frac{dQ}{dS}$ ensures that a positive value of this derivative represents an inflow for a specific salinity class. To obtain TEF values that are less sensitive to the number of salinity bins, which could lead to spurious increases in transport, MacCready et al. (2018) recommended using a dividing salinity (S_{div}), which separates the inflowing higher salinity water from the outflowing lower salinity water. This partitioning is achieved by locating the salinity at which the flux function $q(S)$ transitions from positive (inflow) to negative (outflow) values, or vice versa, corresponding to the extremum of the cumulative transport function $Q(S)$ where its derivative $\frac{dQ}{dS}$ equals zero. Once the dividing salinities have been found, the TEF values can be quantified as,

$$Q_{\mathrm{in}}(S) = \int_{S_{\mathrm{div}}}^{S_{\mathrm{max}}} q dS, \quad Q_{\mathrm{out}}(S) = \int_{S_{\mathrm{min}}}^{S_{\mathrm{div}}} q \, dS. \tag{3}$$

Here, Q_{in} and Q_{out} represent the TEF inflow and outflow volumes at the estuary mouth. Lorenz et al. (2019) further developed this mathematical concept, demonstrating the proper convergence of the dividing salinity method and its applicability to exchange flows with more than two layers. We adopt this approach that includes multi-layered exchange flows termed the 'Extended Dividing Salinity Method', and readers are referred to Lorenz et al. (2019) for more details.

Similarly, the inward and outward salt flux, $Q^S_{\mathrm{in}}(S)$ and $Q^S_{\mathrm{out}}(S)$, are defined as,

$$Q^S_{\mathrm{in}}(S) = \int_{S_{\mathrm{div}}}^{S_{\mathrm{max}}} q^S \, S \, dS, \quad Q^S_{\mathrm{out}}(S) = \int_{S_{\mathrm{min}}}^{S_{\mathrm{div}}} q^S \, S \, dS. \tag{4}$$

Once these are found, the flux-weighted average inflow and outflow salinities can be quantified as,

$$S_{\mathrm{in}} = \frac{Q^S_{\mathrm{in}}}{Q_{\mathrm{in}}}, \quad S_{\mathrm{out}} = \frac{Q^S_{\mathrm{out}}}{Q_{\mathrm{out}}}. \tag{5}$$

10.3389/fmars.2024.1458758

The difference between S_{in} and S_{out} describes the stratification, quantified as the transport-weighted salinities of the exchange flow as,

$$\Delta S = S_{in} - S_{out}. \quad (6)$$

This value of ΔS will be used to understand how stratification in the fjord varies in the dry and typical years as well as to understand how different forcing mechanisms such as tides, wind and river alter stratification during the investigated years. TEF analyses will be carried out in the section located at the mouth of the Reloncaví Fjord.

4 Results

4.1 Trends in precipitation, river inflow, and wind

The MSL pressure and precipitation from the austral summer to fall of 1980 to 2020 in the Reloncaví Fjord area and the Puelo River discharge all revealed trends toward drier conditions (Figure 2). The MSL pressure (Figure 2A) shows a positive trend, indicating that the pressure increases by 0.032hPayear^{-1}, while the precipitation time series indicates that rainfall will decrease by −0.85mmyear^{-1} over the 40-year period (Figure 2B). Most significantly, and likely a product of the decreasing rainfall, river discharge decreases by −10.18m^3 s^{-1} year^{-1} (Figure 2C). These trends have been determined with statistical confidence, as the uncertainties derived from Monte Carlo simulations are smaller than the trend slopes. These results suggest a long-term trend toward drier conditions in the region. We will now consider the monthly variability of the river inflow into Reloncaví Fjord, focusing on the Puelo River, which is the largest contributor of freshwater. The discharge will be considered during the year of the extreme drought, 2016, and the year with more typical precipitation, 2018 (Figure 2B).

The monthly average flow rates of the Puelo River for 2016 and 2018 (Figure 3A) show a decrease during the austral summer months (January-February) followed by a progressive increase from the fall through to spring (April-November) in both years. Despite this overarching trend, differences between the two years are evident. The year 2016, marked by severe drought conditions, showed the lowest flow rates (< 500m^{3}s^{-1}) not just in the summer (January-March) but also spanning the entire fall (April to June) and the beginning of winter (July). Conversely, in 2018, while adhering to the same cyclical pattern as 2016, the discharge values were below 500m^{3}s^{-1} only during the summer months of February and March and were higher than those of 2016 except for the month of August (Figure 3A).

The wind stress reveals yearly differences in intensity and direction, as well as between the years 2016 and 2018. Overall, the east-west wind stress (τ_x) is more intense than the north-south (τ_y) for both years (Figures 3B, C) due to the mountainous terrain surrounding the entrance of the fjord funneling the wind in an east-west orientation (Figure 1). During the summer months (January to March), the east-west wind stress is largely positive (east), and therefore the wind is directed into the fjord. This trend shifts in fall and, more notably, in winter (April to August), when the wind stress is negative (west) and therefore directed out-fjord. However, this is more prevalent in 2018, as the wind velocities in fall and winter of 2016 were overall weak in comparison. Subsequently, in spring (November and December), the direction of the wind stress was again predominantly positive. The north-south component of wind stress (τ_y), although weaker in magnitude than the east-west component, is almost consistently positive throughout both years, indicating a predominantly northward directed wind.

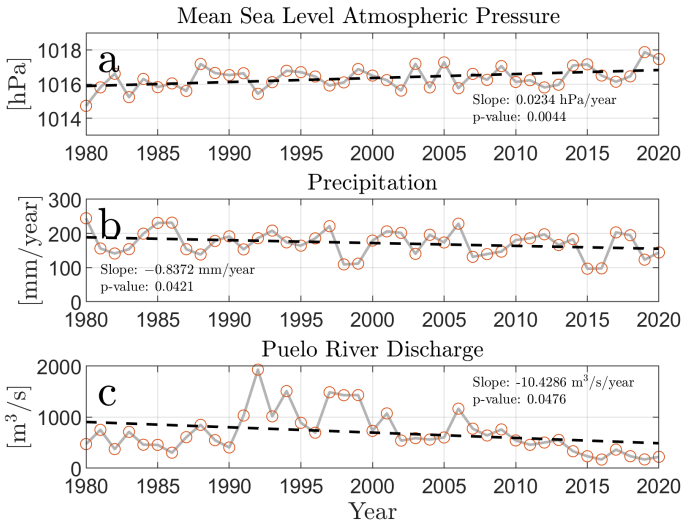

FIGURE 2
Time series of the austral summer (January to March) averages from 1980-2020 for **(A)** Mean Sea Level Atmospheric Pressure [hPa], **(B)** Precipitation [mm/year], and **(C)** discharge from the Puelo River [m^3s^{-1}]. The black dashed line in each subplot denotes the linear trend line. The slope and p-values of these trend lines were determined using linear regression.

10.3389/fmars.2024.1458758

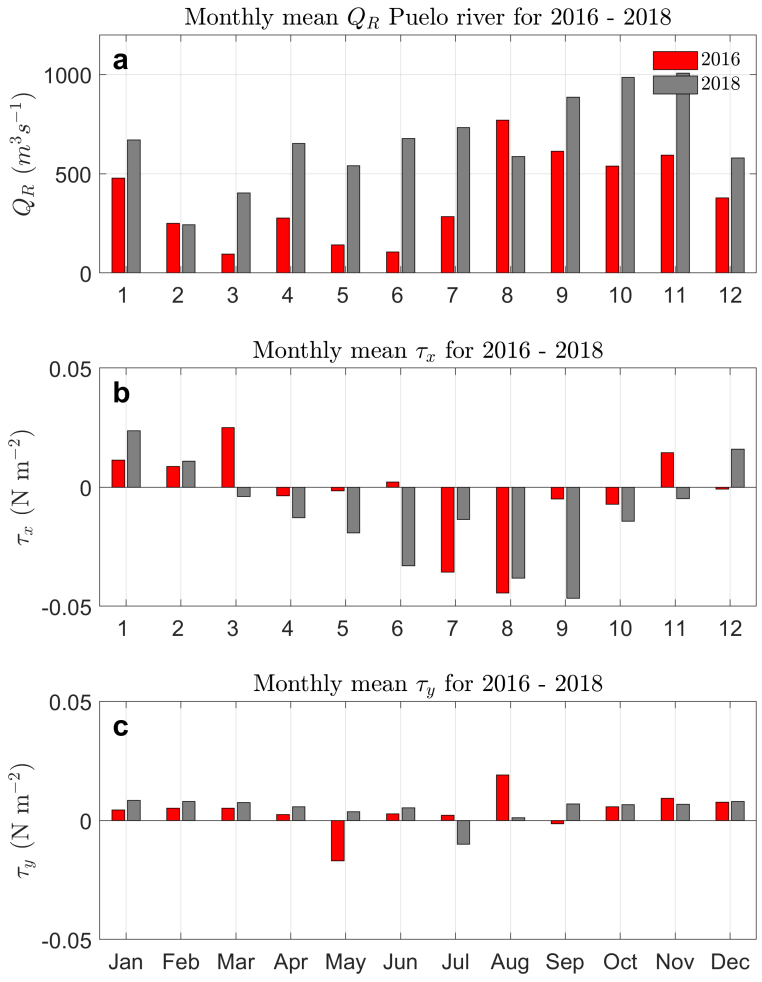

FIGURE 3
Comparison of river discharge and wind stress for 2016 (red) and 2018 (gray). **(A)** The monthly average Puelo River discharge, **(B)** the monthly average east-west wind stress (τ_x), and **(C)** the monthly average north-south wind stress (τ_y).

4.2 Total Exchange Flow (TEF) in 2016 vs. 2018

The Total Exchange Flow (TEF) at the mouth of the Reloncaví Fjord was calculated for the years 2016 and 2018. The first simulation considers forcing from river discharge, wind stress, and tides (RTW-1) (Figure 4). The bulk TEF values were lower in 2016 than 2018 by approximately 14.3% for Q_{in} and 16.7% for Q_{out} (Figure 4). The annual-mean salinity transport with respect to salinity classes, $q^S = \frac{dQ^S}{dS}$, spans higher salinity classes in 2016, with the maximum salinity exceeding 33 g kg^{-1} in 2016 while it remained less than 33 g kg^{-1} in 2018. This suggests that the water column was overall saltier in 2016 than 2018, likely due to the decreased precipitation in the region and decreased freshwater inflow to the fjord, which subsequently weakened the exchange flow.

The tidally averaged yet temporally varying exchange flow values and their associated salinity classes exhibit a dependency on the river inflow, Q_R, in both the ranges of salinity and the strength of the exchange flow (Figures 5A, C, D, F). When river discharge dropped below 500m^{3}s^{-1} for extended periods of time (more than one month), the range of salinities found in the fjord decreased, trending toward higher values. This occurred twice in 2016, namely from mid January to mid April, and May to the start of July with the most limited salinity range being ~ 32–33 g kg^{-1} (Figures 5A, C). In 2018 the river discharge was overall higher and therefore the range of salinities in the fjord was consistently wider and fresher than 2016. There was only one time period, from mid January to early March, when the river discharge fell below 500m^{3}s^{-1} for over one month. During this time period the range of salinity in the fjord was limited to ~ 30–32.7 g kg^{-1} (Figures 5D, F). When river discharge was low in both 2016 and 2018, there were several instances with inflow at both the high and low ends of the salinity range, indicating that the freshest water in the fjord at these times was being advected into the fjord rather than out. This is most pronounced in 2016, particularly in March to early April and in June, however it also occurs in February 2018 although much weaker in comparison to 2016 (Figure 5F).

The influence of wind stress on TEF dynamics is qualitatively less apparent than the river, but could be the cause of the inflow of low salinity waters during low river discharge. This phenomenon may occur when baroclinic forcing is weak, allowing in-fjord wind

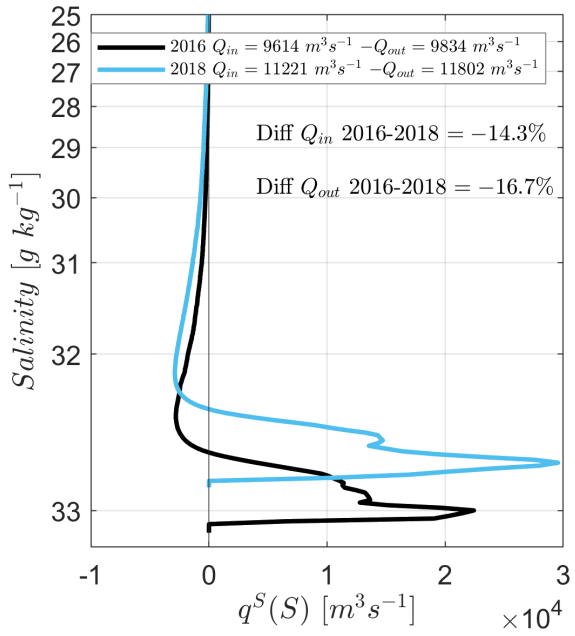

FIGURE 4
Annual-mean salinity transport $q^S(S)$ for 2016 (black line) and 2018 (blue line) with respect to salinity class. The TEF inflow (Q_{in}) and outflow (Q_{out}) values integrated over the salinity bins are given in the legend.

to weaken or reverse the typical near-surface outflow of the estuarine circulation. In fact, during the 'inflow' events, the wind is predominantly directed eastward (in-fjord) with pulses exceeding 0.05 Pa (Figures 5B, E). This will be expanded upon more in the following sections.

4.3 Exchange flow drivers

Temporal variations in TEF outflow, Q_{out}, revealed that river discharge was by far the main driver of the TEF outflow, with the tide the second largest contributor and the wind the third (Figure 6) for both 2016 and 2018. While the ordering of contributing forces remained consistent between the two years, the magnitudes of their contributions differed, suggesting variations in the relative importance of these forces under different conditions. In both years, river discharge was the dominant contributor in all seasons, particularly during winter and spring when TEF was at its peak. The river's contribution to the outflow was 66.2% for 2016 and 73.5% for 2018, while the tidal contribution was 22.1% for 2016 and 17.3% for 2018, never surpassing that of the river. The contribution from wind was most apparent during the summer months in 2016 and in the winter of 2018. The annual average of the wind contribution was 12.3% in 2016 and 9.1% for 2018 (Figure 6).

In 2016, the river's contribution to TEF outflow, albeit still predominant, represented a smaller proportion compared to that of 2018, particularly during the summer and fall seasons, in these periods, the contribution hovered around 62% (62.52% for summer and 62.91% for fall; Figure 6). The reduction in the river's relative contribution allows the influences of wind and tide to emerge more prominently. For example, during periods of low river discharge (< 500 m^3s^{-1} in summer 2016), the wind and tidal contributions to the TEF outflow increased to ~ 16 and 21%, respectively, Figure 6A), compared to the same season in 2018 when wind contributed 13% and tide contributed 15% to TEF outflow (Figure 6B). This implies that when river discharge is weak, higher-frequency forcing can augment, inhibit, or attenuate TEF. For example, in the tide only simulation (difference between RT-2 and R-3), the TEF outflow

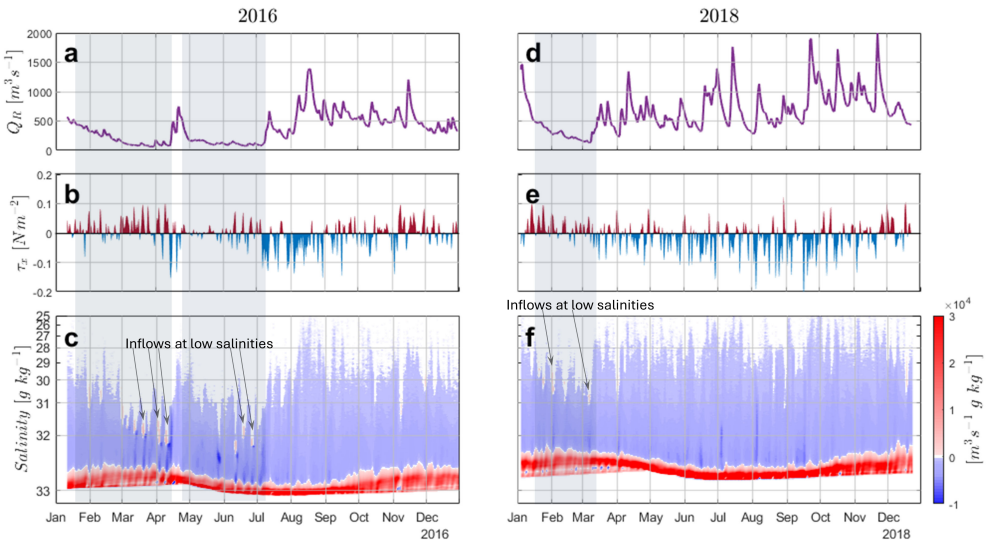

FIGURE 5
(A) Time series of daily river discharge Q_R, **(B)** the east-west wind stress with positive values denoting an in-fjord wind stress and negative values denoting out-fjord wind stress, and **(C)** the tidallyaveraged TEF salinity profile for 2016 with positive values denoting inflow and negative values denoting outflow. Subplots **(D-F)** are the same as **(A-C)** but for 2018. The transparent gray boxes represent times when the river discharge was under 500m^3s^{-1}. The arrows show instances of inflow at low salinities found only when river discharge was low.

10.3389/fmars.2024.1458758

oscillates at a fortnightly periodicity (Figure 6 and Wavelet details in Supplementary Figures S6C, G in the Supplementary Material). Wind, on the other hand, alters the TEF outflow at even higher frequencies in the ~ 5–10 day synoptic band (Supplementary Figures S6B, F) such that wind influence can surpasses that of tides and river on short temporal scales, even with minor wind changes (<0.05-0.1 Pa). This aspect will be explored further in the following section.

4.4 Wind effects on TEF, salinity, and circulation

Despite the surface wind being a secondary factor in the dynamics of the Total Exchange Flow (TEF), its role becomes important under specific circumstances, notably during periods of minimal river discharge (<500 $m^3 s^{-1}$), such as was observed in the summer and early fall of 2016. We examined the exchange flow over approximately 40 days during this period to analyze the exchange flow compared to wind variability, near-surface salinity, and the vertical subtidal flow structure at the mouth of the fjord (Figure 7). In-fjord (eastward) wind pulses occurred every ~ 5–10 days while the river discharge was sustained below < 500 $m^3 s^{-1}$ (Figure 7A). The in-fjord wind influenced the exchange flow by mixing the near-surface layer and advecting the fresher surface water into the fjord (Figure 7). In addition, the TEF outflow was augmented at mid-range salinities during the pulses, which translated as augmented subtidal outflow at deeper depths which is found, for example, on March 1st, 6th, 12th, 20th, 25th, April 3rd and most pronounced on April 9th (Figure 7D). Once the in-fjord wind relaxed, the TEF outflow was enhanced at the mid to lower salinity bins as stratification in the near-surface layers was re-established.

The intricate interplay between river and wind influence demonstrates how specific wind patterns can alter fjord dynamics by promoting vertical mixing and modifying the salinity profile and current structure, but only under certain hydrological regimes. This emphasizes the nuanced and situational impact of wind on fjord ecosystems during critical periods of low river discharge. In fact, in years with more typical river discharge, such as 2018, the wind was not able to influence TEF to such a degree (Figure 5F). The summer months of 2016 were when the devastating harmful algal bloom was present in Northern Patagonia, implying that parameters such as these could be indicators as to when the fjord ecosystem will be susceptible to hazards such as harmful algal blooms. This will be considered further in the discussion section. First, the influence of the different forcing mechanisms (river, tide, and wind) on stratification will be investigated.

4.5 Stratification

When comparing stratification conditions between 2016 and 2018, the latter year generally exhibits higher ΔS values, indicating a more stratified water column (Figure 8). To elucidate the roles of tides and wind on destratification processes in the fjord, we investigated how ΔS changes depending on the river, tide, and wind forcing. Seasonal variations in ΔS were found in all simulations, influenced by seasonal variations in river inputs, which were most pronounced during the high runoff periods in winter and spring (July to December). When considering the model output that included only river input (R-3, red lines in Figure 8), this simulation resulted in the most stratified conditions for both years.

In the simulation that includes both rivers and tide effects (RT-2, blue line in Figure 8), ΔS still varies along with the river flow seasonal cycles, however, stratification is decreased from that of the river-only case (R-3). Focusing on 2016, from summer to fall (January to July), tides decreased stratification by ~ 1 g kg^{-1}, however, during winter and spring, when river discharge values were at their peak, the tides were able to decrease stratification by nearly 3 g kg^{-1}. This is not a surprise as the more freshwater available to mix, the more effective the tides are at mixing.

Comparing the model output that included river and tides (RT-2, blue line) to the output with all forcing considered (RTW-1, black line) allows us to assess the additional impact of wind on the destratification in addition to the tide (Figure 8). In both 2016 and 2018, the wind was largely found to attenuate the stratification although in some instances it did slightly enhance stratification. This observation suggests that the

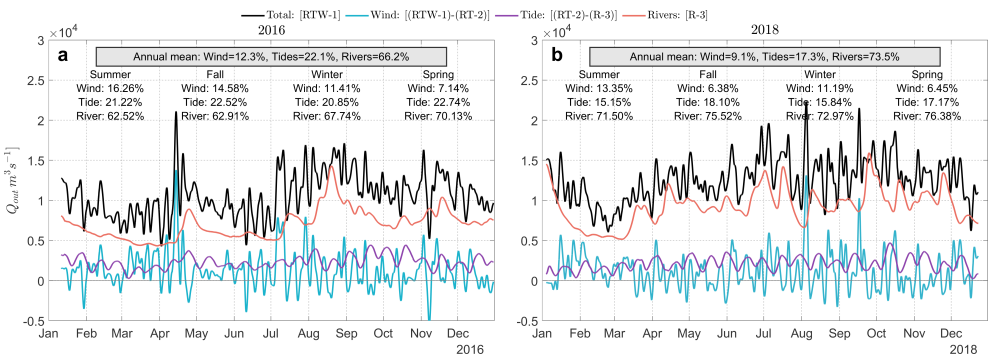

FIGURE 6
Temporal variations in TEF outflow Q_{out} contributions in the Reloncaví Fjord Mouth for **(A)** 2016 and **(B)** 2018. The plots illustrate the comparative monthly outflow volumes (Q_{out}), categorized by the driving forces: Total (black line), Wind (teal line), Tide (purple line), and River (orange line). Seasonal annotations provide the percentage contributions of wind, tide, and river forces.

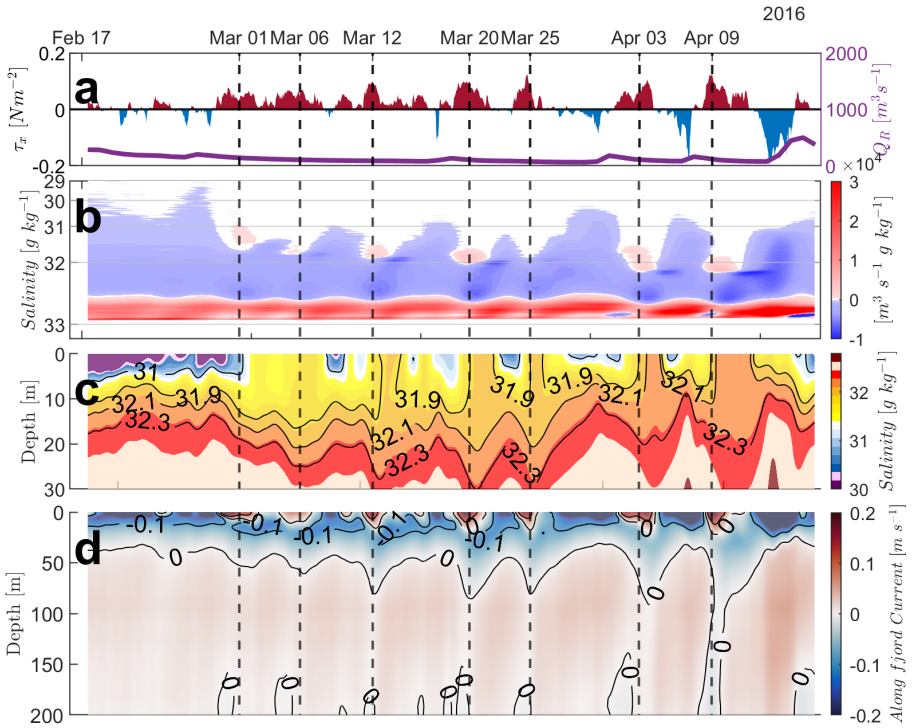

FIGURE 7
Time series at the Reloncaví Fjord mouth during the end of summer and early fall (2016) to investigate the influence of wind forcing. **(A)** The east-west wind stress, τ_x, and river discharge, Q_R. **(B)** The TEF with respect to salinity bins. **(C)** Subtidal salinity profile from the surface to 30 m depth. **(D)** Subtidal current velocities at the fjord's mouth. Negative values denote outflow and positive values denote inflow. The vertical dashed lines indicate times when both the river discharge is below 500 m^3/s and the wind is directed in-fjord.

wind's direction, aligning with or opposing the baroclinic pressure gradient, affects stratification. During the summer and fall of 2016 in particular, the period characterized by very low river discharge (< 500 $m^3 s^{-1}$), the in-fjord winds, though still relatively weak, led to a discernible escalation in destratification that nearly homogenized the water column (Figure 8A March and June). Moreover, the wind's effect operates at higher frequencies compared to the other forcing factors (tides and river). While these high-frequency wind events during low river discharge conditions might not have a significant impact on annual scales, they can be critical over short time periods. Such events can alter the fjord's physical and biogeochemical structure for several days, potentially affecting the local ecosystem dynamics, particularly with rapidly developing harmful algal blooms (HABs). We will now discuss the results of this study, extrapolating our findings to explore whether historical river discharge and stratification conditions can be used as indicators of hazardous conditions in the Reloncaví Fjord, particularly concerning HABs.

5 Discussion

As climate change continues to reshape global weather patterns, its impact on regional hydrological cycles is becoming increasingly evident, particularly in environments such as Northern Patagonia. The 2016 drought in Patagonia offers a case study of these impacts, serving as a potential harbinger of future conditions under more frequent and severe climate-driven hydrological anomalies as documented by Aguayo et al. (2019). In this context, our investigation into the Total Exchange Flow (TEF) dynamics within the Reloncavi Fjord during such an extreme event reveals insights into the balance between freshwater inputs and other physical drivers, such as wind and tides, in determining the overall exchange with the adjacent ocean.

Our results delineate the varying impacts of river discharge, tides, and wind on the fjord's hydrodynamics, with river flow consistently identified as the dominant force, particularly during winter and spring (JulyDecember). In the austral summer and fall of 2016, the dominance of river flow diminished due to the drought conditions, allowing for wind and tidal forces to destratify the water column, reduce TEF, and periodically reverse the typical estuarine circulation structure. Is it a coincidence that 2016, which coincided with one of the strongest harmful algal bloom (HAB) events on record in the Northern Patagonian Fjords (resulting in up to USD 800 million in losses to salmon aquaculture, according to GlobalHAB, 2023), also saw reduced river discharge and destratification? We will now attempt to determine if there are links between historical instances of these conditions and other documented HABs in the region.

While river discharge is the primary driver of TEF in Reloncaví Fjord, wind can influence the dynamics over much shorter temporal scales (5-10 days, Figure 7; Supplementary Figure S6). Our results have shown that during periods of low river discharge, even weak wind events can cause the stratified upper layer to mix, indicating that dense subsurface waters can reach the surface (Figure 7),

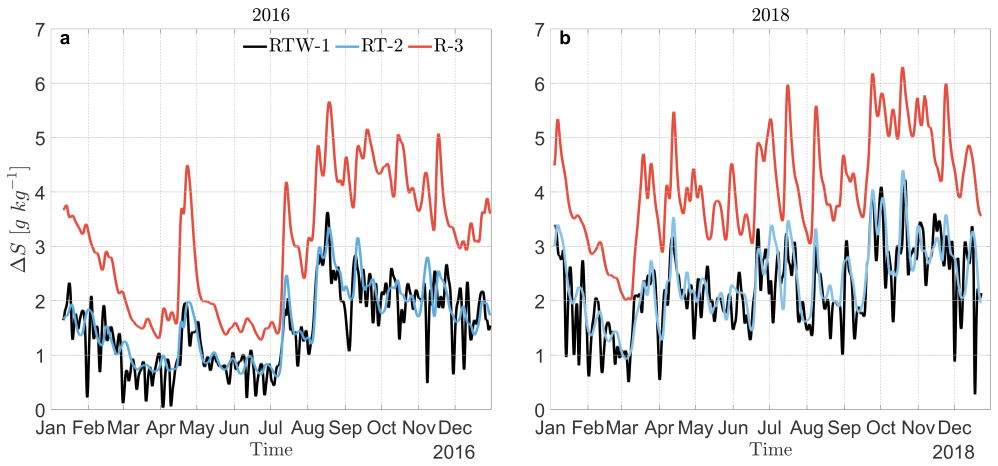

FIGURE 8
Temporal variation of stratification ΔS ($S_{in} - S_{out}$) over the years **(A)** 2016 and **(B)** 2018. The black line represents ΔS including river, tide, and wind as forcing mechanisms (RTW-1 case), the blue line includes river and tides only (RT-2 case), and the red line includes only river contributions (R-3 case).

allowing chemical tracers such inorganic nutrients to reach the surface layer, potentially altering the fjord's ecological balance, as suggested by the findings of León-Muñoz et al. (2018) during the 2016 HAB event in North Patagonia. In the Strait of Georgia, a semi-enclosed estuarine area in Canada, Moore-Maley and Allen (2022), used a high-resolution biophysical coupled model to demonstrate that wind-driven upwelling plays a crucial role in controlling surface nutrients and water properties. They showed how episodic upwelling, steered by mountainous topography and influenced by prevailing wind patterns, can produce significant positive nitrate anomalies along the shores. At the head of the Comau Fjord, upwelling conditions were also reported due to wind influence and contributed to the injection of nutrients and other biogeochemical parameters into the surface layer (Crosswell et al., 2022; Díaz et al., 2023). In a study by Díaz et al. (2023), upwelling was produced by dominant southern wind which uplifted deep water rich in nutrients and organic matter. This was proposed as the main mechanism generating a HAB event of Heterosigma akashiwo in the Comau Fjord during the autumn 2021.

These findings suggest that wind-driven processes may play a role in nutrient dynamics and the formation of HABs under specific river flow conditions. However, predicting HAB occurrences still presents a formidable challenge due to the complex interplay of eco-physiological factors and physical and chemical processes (Berdalet et al., 2016), including variations in salinity, temperature, light and nutrient availability, all of which favor different species. Our understanding of these processes that control HAB dynamics in general is incomplete, making their parameterization in numerical models extremely difficult (Berdalet et al., 2016). The intricate nature of these interactions not only hinders the development of decision support tools for effective management and regulation but also highlights the difficulty of generalizing predictive models for HAB occurrences due to the unique conditions each algal species require. Our study found that low-river discharge conditions permit wind forcing to destratify the upper water column, allowing for any present subsurface biochemical conditions (typically found below the pycnocline) to reach the surface. Therefore, a potential indicator for HABs in general, independent of species specific conditions, could be fjord stratification conditions. Therefore, we investigate whether variations in river discharge and the ensuing changes in stratification conditions could serve as a reliable and easily quantifiable proxy for HABs decision support and forecasting.

5.1 Stratification as an indicator for HABs

Wind, river discharge, and stratification interact to shape the exchange flow, with low river discharge conditions driving destratification. This destratification (low ΔS) could play a significant role in the ecosystem's response to environmental conditions, influencing the likelihood of HAB events. In this context, while the correlation between winds and exchange flow during low discharge conditions remains an essential aspect of our analysis, it is clear that river discharge has a more direct relationship with stratification.

To explore the relationship between stratification and harmful algal blooms (HABs), we conducted a statistical analysis correlating reconstructed stratification levels (ΔS) from 1980 to 2021 with documented HAB events. The initial correlation between river discharge and stratification in the Reloncaví Fjord was established using data from 2016 and 2018 (Figure 9). Following this, we reconstructed long-term stratification conditions using the river flow data from the FLOW-IFOP model (described in Section 3.1) over the period 1980 to 2021. For each year, the seasonal stratification index (ΔS) was calculated for all four seasons (summer, fall, winter, spring), allowing for a comprehensive analysis of long-term trends. This analysis was paired with a logistic regression model (Ralston and Moore, 2020; Lane et al., 2009), which evaluated how different stratification levels influenced the probability of specific HAB species occurrences.

The results of this analysis (Figure 10) demonstrated that Pseudchatonella spp. is strongly associated with low stratification

levels, particularly during the summer months when river discharge is reduced, leading to destratification (Figure 10A). The statistical model revealed a significant inverse relationship between ΔS and HAB occurrence for this species, with the probability of occurrence exceeding 50% when stratification levels were low (p-value < 0.05). Notably, when focusing on the post-1990 period, which includes more comprehensive monitoring records, the probability of occurrence increased to 68% (Figure 10B). These findings support the hypothesis that low-discharge-induced destratification fosters conditions favorable for Pseudchatonella spp. blooms, consistent with prior research that links salinity fluctuations to the proliferation of this ichthyotoxic species (Mardones et al., 2019).

In fall and winter, no significant relationships with any species were observed, with p-values greater than 0.05 (Figures 10C–F). This suggests that during these seasons, stratification levels may not play a dominant role in driving the occurrence of harmful algal blooms.

In contrast, the relationship for Alexandrium catenella presented a different pattern. This species was more closely associated with periods of high stratification during the spring, a season characterized by increased river discharge (Figure 10G). The logistic regression model confirmed a positive relationship between higher stratification and the occurrence of Alexandrium catenella blooms, suggesting that these conditions may contribute to the species' ability to thrive during this period (Figure 10H).

While Pseudchatonella spp. and Alexandrium catenella showed clear relationships with stratification levels, other species examined in this analysis did not exhibit significant patterns, with p-values greater than 0.05. This suggests that, for these species, stratification alone may not be a primary driver of bloom occurrences, and additional environmental factors may play a more critical role.

Overall, our findings emphasize the significant role that seasonal changes in river discharge play in shaping stratification dynamics in the fjord and how these dynamics influence the occurrence of specific HAB species. Low-discharge-induced destratification in summer is strongly linked to the occurrence of Pseudchatonella spp., while high-discharge-induced stratification during spring is linked to Alexandrium catenella blooms. However, we do not claim to present a mechanistic explanation for the bloom generation process; rather, our analysis provides insights into which species are associated with varying degrees of stratification.

Further research is necessary to explore the complex interactions between environmental factors and HABs, especially considering other influences such as nutrient availability, climatic indices like ENSO, and larger-scale oceanographic changes. Nevertheless, this study contributes valuable insights into the dynamics of HABs in Patagonian fjords and underscores the importance of stratification as a key environmental factor influencing the distribution and frequency of these blooms.

5.2 Study limitations

The configuration and validation of our model have been crucial in examining exchange flow dynamics and stratification within the Reloncaví Fjord. Although the model successfully reproduces the general stratification structure of the fjord (see Supplementary Material), it is not a perfect representation. There is an inherent loss of stratification due to diffusion or numerical mixing. Limited measurements during the modeling period do not allow for extensive evaluation of the model's performance in space and time. Furthermore, the atmospheric model with a 3 km resolution is likely insufficient to capture the intricacies of wind patterns within the fjord, characterized by its steep and complex topography. Therefore, there is some uncertainty in using the atmospheric model, but now there are no higher-resolution data sources available and we believe that the validation shows that the model can accurately capture long-term variability, which was the focus of the present study.

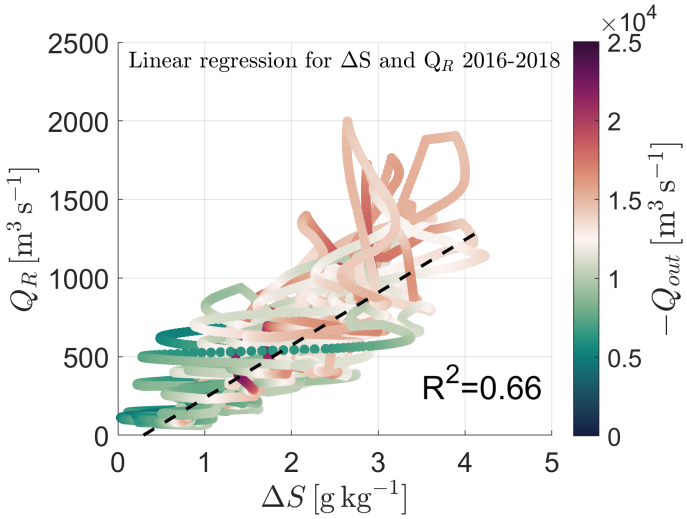

FIGURE 9
Correlation between river discharge Q_R and stratification ΔS for 2016 and 2018 combined. The black lines are the linear regression lines with the R^2 value. The color gradient represents the magnitude of TEF volume outflow, Q_{out}.

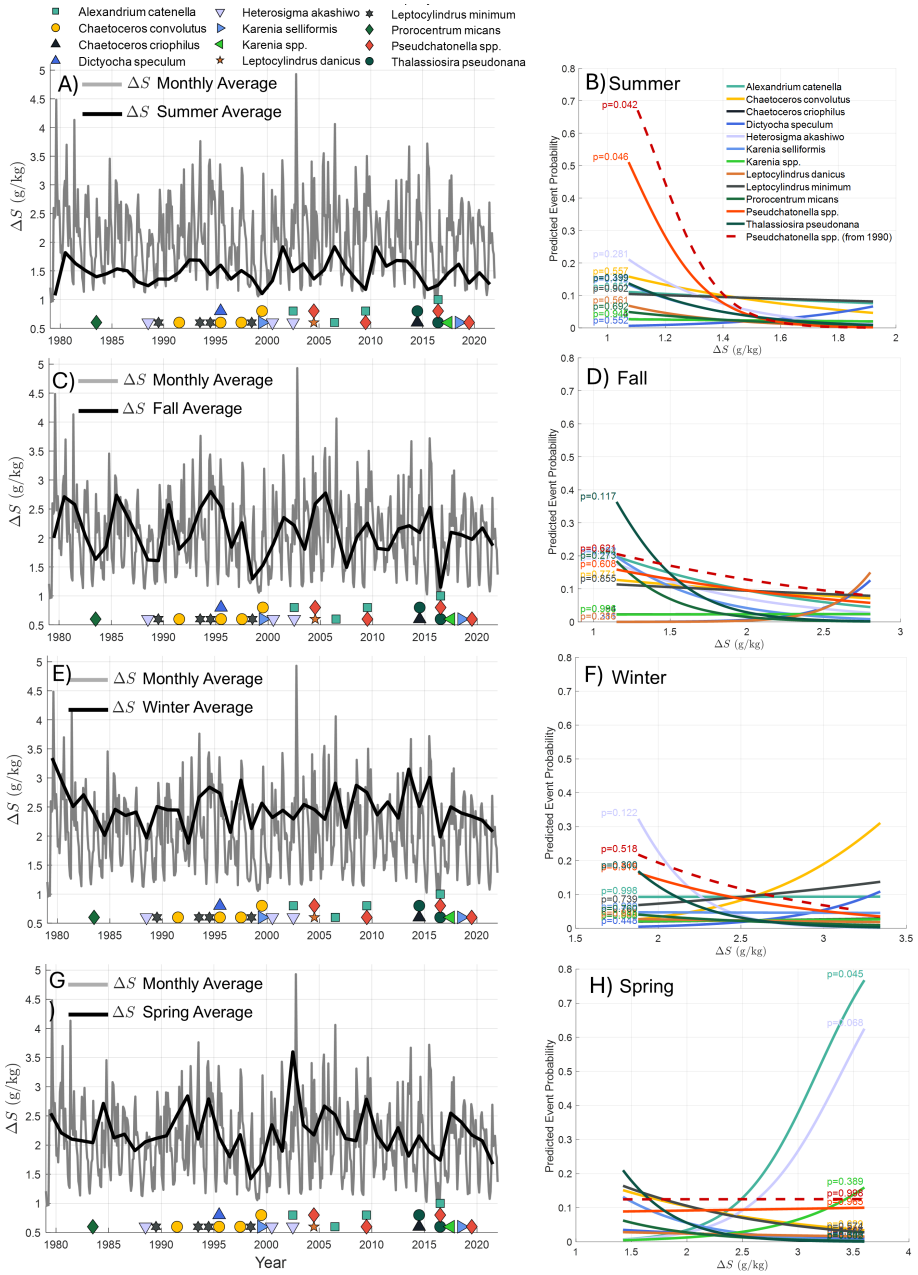

FIGURE 10
Reconstructed stratification index ΔS and its relationship with harmful algal blooms (HABs) from 1980 to 2021. **(A, C, E, G)** show monthly averages (gray line) of ΔS alongside seasonal averages (black line) for summer, fall, winter, and spring, respectively. HAB events are represented by different symbols and colors corresponding to the species involved, indicating the presence of blooms for each year. **(B, D, F, H)** display logistic regression models that assess the probability of HAB occurrence for each species as a function of the stratification index. A significant inverse relationship is found for Pseudchatonella spp. during summer months **(B)**, where low ΔS (destratification) is linked to a higher probability of occurrence (p-value < 0.05). In contrast, Alexandrium catenella shows a positive relationship with higher stratification (increased ΔS) during spring **(H)**. Other species display weaker or nonsignificant relationships, indicating that stratification alone may not fully explain their occurrence.

Another potential concern is that the R-3 model simulation intends to focus solely on river inputs, but it also includes changes to the offshore boundary salinity conditions. The variation in ocean salinity generates horizontal salinity gradients that are not associated with river-induced variability. We do believe that these variations are small compared to the river input, particularly in Reloncavi Fjord. However, future research should evaluate the influence of offshore salinity variability on TEF and stratification in fjord regions. In addition to improving numerical models, increasing *in-situ* observations, such as networks of oceanographic buoys, is also necessary. These will contribute to the future understanding of the natural and anthropogenic processes that affect Patagonian fjords.

6 Conclusion

Our research on the Total Exchange Flow (TEF) dynamics in the Reloncaví Fjord, particularly under the severe drought conditions of 2016, uncovers a complex interaction among freshwater inputs, wind, and tidal forces that influence estuarine exchange processes. Results showed the crucial role of river discharge in shaping the fjord's annual exchange flow dynamics, while also highlighting the significant, albeit more transient, impact of wind in modulating subsurface water dynamics. Findings suggest that in 2016, when precipitation and river discharge were reduced due to drought conditions, wind and tidal effects played a more dominant role. Wind mixing was able to destratify the upper water column, enabling subsurface saltier waters and their associated biogeochemical conditions to reach the surface. Moreover, in 2018, when river discharge and precipitation were more typical, TEF results responded to river discharge and were less sensitive to higher-frequency wind forcing.

Additionally, our statistical analysis linking river discharge, wind forcing, and stratification ΔS with harmful algal blooms (HABs) highlighted the susceptibility of the fjord to HAB events under certain conditions. Using logistic regression models, we found a significant inverse relationship between ΔS and the occurrence of Pseudchattonella spp. blooms during the summer. Low stratification levels, indicative of destratification due to reduced river discharge, were associated with a higher probability of HAB events for this species. Conversely, Alexandrium catenella blooms were more strongly linked to higher stratification levels during the spring, reflecting the influence of increased freshwater input.

Data availability statement

The raw data supporting the conclusions of this article will be made available by the authors, without undue reservation.

Author contributions

EP: Conceptualization, Data curation, Formal analysis, Investigation, Methodology, Resources, Software, Validation, Visualization, Writing – original draft, Writing – review & editing. LR: Conceptualization, Formal analysis, Funding acquisition, Investigation, Methodology, Project administration, Resources, Supervision, Validation, Writing – original draft, Writing – review & editing. IP-S: Conceptualization, Formal analysis, Funding acquisition, Investigation, Methodology, Project administration, Resources, Supervision, Validation, Writing – original draft, Writing – review & editing.

Funding

The author(s) declare financial support was received for the research, authorship, and/or publication of this article. This research was supported by the National Science Foundation under Grant No. 2045866. The authors extend their gratitude to the Chonos Initiative of the Instituto de Fomento Pesquero (IFOP), Chile for providing access to its computational resources, enabling the use of the MIKE 3, WRF, and FLOW models for this study. IP-S was also funded by FONDECYT 1211037, COPAS COASTAL FB210021, and CIEP R20F002. LR also received a Fulbright U.S. Scholar grant during the research that led to this publication.

Acknowledgments

Special thanks are also extended to Manuel Castillo for facilitating CTD and tide gauge data used for the validation of the hydrodynamic model.

Conflict of interest

The authors declare that the research was conducted in the absence of any commercial or financial relationships that could be construed as a potential conflict of interest.

Publisher's note

Supplementary material

The Supplementary Material for this article can be found online at: https://www.frontiersin.org/articles/10.3389/fmars.2024.1458758/full#supplementary-material

References

Aguayo, R., León-Muñoz, J., Vargas-Baecheler, J., Montecinos, A., Garreaud, R., Urbina, M., et al. (2019). The glass half-empty: climate change drives lower freshwater input in the coastal system of the Chilean northern patagonia. *Climatic Change* 155, 417–435. doi: 10.1007/s10584-019-02495-6

Aiken, C. M. (2008). Barotropic tides of the Chilean inland sea and their sensitivity to basin geometry. *J. Geophysical Research: Oceans* 113 (C8), C08024. doi: 10.1029/2007JC004593

Arneborg, L., Erlandsson, C. P., Liljebladh, B., and Stigebrandt, A. (2004). The rate of inflow and mixing during deep-water renewal in a sill fjord. *Limnology Oceanography* 49, 768–777. doi: 10.4319/lo.2004.49.3.0768

Aure, J., Molvær, J., and Stigebrandt, A. (1996). Observations of inshore water exchange forced by a fluctuating offshore density field. *Mar. pollut. Bull.* 33, 112–119. doi: 10.1016/S0025-326X(97)00005-2

Bedriñana-Romano, L., Viddi, F. A., Artal, O., Pinilla, E., and Hucke-Gaete, R. (2023). First estimate of distribution, abundance, and risk of encounter with aquaculture vessels for the rare Chilean dolphin in the entire northern Chilean patagonia. *Aquat. Conservation: Mar. Freshw. Ecosyst.* 33, 1535–1551. doi: 10.1002/aqc.4012

Berdalet, E., Fleming, L. E., Gowen, R., Davidson, K., Hess, P., Backer, L. C., et al. (2016). Marine harmful algal blooms, human health and wellbeing: challenges and opportunities in the 21st century. *J. Mar. Biol. Assoc. United Kingdom* 96, 61–91. doi: 10.1017/S0025315415001733

Boisier, J. (2023). *Cr2met: A high-resolution precipitation and temperature dataset for the period 1960–2021 in continental Chile (Zenodo)*. doi: 10.5281/zenodo.7529681

Buchan, S. J., Rendell, L. E., and Hucke-Gaete, R. (2010). Preliminary recordings of blue whale (balaenoptera musculus) vocalizations in the gulf of corcovado, northern patagonia, Chile. *Mar. Mammal Sci.* 26, 451–459. doi: 10.1111/j.1748-7692.2009.00338.x

Burchard, H., Bolding, K., Feistel, R., Gräwe, U., Klingbeil, K., MacCready, P., et al. (2018). The knudsen theorem and the total exchange flow analysis framework applied to the baltic sea. *Prog. Oceanography* 165, 268–286. doi: 10.1016/j.pocean.2018.04.004

Cáceres, M., Valle-Levinson, A., and Atkinson, L. (2003). Observations of cross-channel structure of flow in an energetic tidal channel. *J. Geophysical Research: Oceans* 108 (C4), 108. doi: 10.1029/2001JC000968

Castillo, M. I., Pizarro, O., Cifuentes, U., Ramirez, N., and Djurfeldt, L. (2012). Subtidal dynamics in a deep fjord of southern Chile. *Continental Shelf Res.* 49, 73–89. doi: 10.1016/j.csr.2012.09.007

Crosswell, J. R., Bravo, F., Pérez-Santos, I., Carlin, G., Cherukuru, N., Schwanger, C., et al. (2022). Geophysical controls on metabolic cycling in three patagonian fjords. *Prog. Oceanography* 207, 102866. doi: 10.1016/j.pocean.2022.102866

Cui, X., Mucci, A., Bianchi, T. S., He, D., Vaughn, D., Williams, E. K., et al. (2022). Global fjords as transitory reservoirs of labile organic carbon modulated by organo-mineral interactions. *Sci. Adv.* 8, eadd0610. doi: 10.1126/sciadv.add0610

Danish Hydraulic Institute (DHI) (2019). *MIKE 3 User Guide and Reference Manual* (Denmark: Danish Hydraulic Institute).

Díaz, P. A., Pérez-Santos, I., Basti, L., Garreaud, R., Pinilla, E., Barrera, F., et al. (2023). The impact of local and climate change drivers on the formation, dynamics, and potential recurrence of a massive fish-killing microalgal bloom in patagonian fjord. *Sci. Total Environ.* 865, 161288. doi: 10.1016/j.scitotenv.2022.161288

Engqvist, A., and Omstedt, A. (1992). Water exchange and density structure in a multi-basin estuary. *Continental Shelf Res.* 12, 1003–1026. doi: 10.1016/0278-4343(92)90013-A

Food and Agriculture Organization of the United Nations (FAO) (2022). *The State of World Fisheries and Aquaculture 2022: Towards Blue Transformation. Tech. rep* (Rome, Italy: FAO). doi: 10.4060/cc0461en

Garreaud, R. D. (2018). Record-breaking climate anomalies lead to severe drought and environmental disruption in western patagonia in 2016. *Climate Res.* 74, 217–229. doi: 10.3354/cr01505

Geyer, W. R., and Ralston, D. K. (2012). (2011). "The dynamics of strongly stratified estuaries," in *Treatise on estuarine and coastal science, vol 2.* Eds. E. Wolanski and D. S. Wolanski (Waltham: Academic Press), 37–51. doi: 10.1016/B978-0-12-374711-2.00206-0

Giddings, S. N., and MacCready, P. (2017). Reverse estuarine circulation due to local and remote wind forcing, enhanced by the presence of along-coast estuaries. *J. Geophysical Research: Oceans* 122, 10184–10205. doi: 10.1002/2016JC012479

Hucke-Gaete, R., Osman, L. P., Moreno, C. A., Findlay, K. P., and Ljungblad, D. K. (2004). Discovery of a blue whale feeding and nursing ground in southern Chile. Proceedings of the Royal Society of London. *Ser. B: Biol. Sci.* 271, S170–S173. doi: 10.1098/rsbl.2003.0132

Ianniello, J. P. (1977). Tidally induced residual currents in estuaries of constant breadth and depth. *J. Mar. Res.* 35 (4). Available online at: https://elischolar.library.yale.edu/journal_of_marine_research/1418.

Inall, M. E., and Gillibrand, P. A. (2010). The physics of mid-latitude fjords: a review. *Geological Society London Special Publications* 344, 17–33. doi: 10.1144/sp344.3

Landaeta, M. F., Gómez, A., Contreras, J. E., Figueroa-González, Y., Pinilla, E., Reche, P., et al. (2023). Linking shape and growth in young-of-the-year rockfish: an ecological carry-over effect? *Mar. Biol.* 170, 103. doi: 10.1007/s00227-023-04248-7

Lane, J. Q., Raimondi, P. T., and Kudela, R. M. (2009). Development of a logistic regression model for the prediction of toxigenic pseudo-nitzschia blooms in monterey bay, california. *Mar. Ecol. Prog. Ser.* 383, 37–51. doi: 10.3354/meps07999

Lange, X., Klingbeil, K., and Burchard, H. (2020). Inversions of estuarine circulation are frequent in a weakly tidal estuary with variable wind forcing and seaward salinity fluctuations. *J. Geophysical Research: Oceans* 125 (9), e2019JC015789. doi: 10.1029/2019JC015789

Lara, A., Urrutia, R., Villalba, R., Luckman, B., Soto, D., Aravena, J., et al. (2005). The potential use of tree-rings to reconstruct streamflow and estuarine salinity in the valdivian rainforest eco-region, Chile. *Dendrochronologia* 22, 155–161. doi: 10.1016/j.dendro.2005.04.002

Launder, B., and Spalding, D. (1974). The numerical computation of turbulent flows. *Comput. Methods Appl. Mechanics Eng.* 3, 269–289. doi: 10.1016/0045-7825(74)90029-2

León, J. E. (2005). *Influencia del caudal del Río Puelo, sobre la salinidad y la concentración de oxígeno disuelto en el estuario de Reloncaví, LLanquihue, Chile*. Tesis de Magíster (Valdivia, Chile: Universidad Austral de Chile), 74 p.

León-Muñoz, J., Urbina, M. A., Garreaud, R., and Iriarte, J. L. (2018). Hydroclimatic conditions trigger record harmful algal bloom in western patagonia (summer 2016). *Sci. Rep.* 8, 1330. doi: 10.1038/s41598-018-19461-4

Linford, P., Pérez-Santos, I., Montero, P., Díaz, P., Aracena, C., Pinilla, E., et al. (2023). Oceanographic processes favoring deoxygenation inside patagonian fjords. *EGUsphere* 2023, 1–34. doi: 10.5194/egusphere-2023-706

Lorenz, M., Klingbeil, K., MacCready, P., and Burchard, H. (2019). Numerical issues of the total exchange flow (tef) analysis framework for quantifying estuarine circulation. *Ocean Sci.* 15, 601–614. doi: 10.5194/os-15-601-2019

MacCready, P. (2011). Calculating estuarine exchange flow using isohaline coordinates. *J. Phys. Oceanography* 41, 1116–1124. doi: 10.1175/2011JPO4517.1

MacCready, P., Geyer, W. R., and Burchard, H. (2018). Estuarine exchange flow is related to mixing through the salinity variance budget. *J. Phys. Oceanography* 48, 1375–1384. doi: 10.1175/JPO-D-17-0266.1

Mardones, J. I. (2020). Screening of Chilean fish-killing microalgae using a gill cell-based assay. *Latin Am. J. Aquat. Res.* 48, 329–335. doi: 10.3856/vol48-issue2-fulltext-2400

Mardones, J. I., Fuenzalida, G., Zenteno, K., Alves-de Souza, C., Astuya, A., and Dorantes-Aranda, J. J. (2019). Salinity-growth response and ichthyotoxic potency of the Chilean pseudochattonella verruculosa. *Front. Mar. Sci.* 6, 24. doi: 10.3389/fmars.2019.00024

Mardones, J. I., Paredes, J., Godoy, M., Suarez, R., Norambuena, L., Vargas, V., et al. (2021). Disentangling the environmental processes responsible for the world's largest farmed fish-killing harmful algal bloom: Chil. *Sci. Total Environ.* 766, 144383. doi: 10.1016/j.scitotenv.2020.144383

Moore-Maley, B., and Allen, S. E. (2022). Wind-driven upwelling and surface nutrient delivery in a semi-enclosed coastal sea. *Ocean Sci.* 18, 143–167. doi: 10.5194/os-18-143-2022

Niemeyer, H., and Cereceda, P. (1984). *Hidrografía* (Instituto Geográfico Militar).

Pérez-Santos, I., Díaz, P. A., Silva, N., Garreaud, R., Montero, P., Henríquez-Castillo, C., et al. (2021). Oceanography time series reveals annual asynchrony input between oceanic and estuarine waters in patagonian fjords. *Sci. Total Environ.* 798, 149241. doi: 10.1016/j.scitotenv.2021.149241

Pinilla, E., Soto, G., Soto-Riquelme, C., Venegas, O., Salas, P., and Cortes, J. (2020). *Determinación de las Escalas de Intercambio de Agua en Fiordos y Canales de la Región de Los Lagos y Región de Aysén del General Carlos Ibáñez del Campo. Tech. rep* (Valparaíso, Chile: Instituto de Fomento Pesquero (IFOP). doi: 10.13140/RG.2.2.17813.65762

Ralston, D. K., and Moore, S. K. (2020). Modeling harmful algal blooms in a changing climate. *Harmful Algae* 91, 101729. doi: 10.1016/j.hal.2019.101729

Reche, P., Artal, O., Pinilla, E., Ruiz, C., Venegas, O., Arriagada, A., et al. (2021). Chonos: Oceanographic information website for Chilean patagonia. *Ocean Coast. Manage.* 208, 105634. doi: 10.1016/j.ocecoaman.2021.105634

Rodi, W. (1984). *Turbulence Models and their Applications in Hydraulics-a State-of-the-Art Review*. International Association for Hydraulic Research.

Shan, S., Hannah, C. G., and Wu, Y. (2019). Coupling of estuarine circulations in a network of fjords. *J. Geophysical Research: Oceans* 124, 6809–6830. doi: 10.1029/2018JC014924

Sibson, R. (1981). "A brief description of natural neighbor interpolation," in *Interpreting multivariate data*. Ed. V. Barnett (New York: John Wiley & Sons), 21–36.

Skamarock, W. C., Klemp, J. B., Dudhia, J., Gill, D. O., Barker, D. M., Duda, M. G., et al. (2008). A description of the advanced research Wrf Version 3, Vol. 475. *NCAR Technical Note NCAR/TN-475+STR. Mesoscale and Microscale Meteorology Division.* (Boulder, Colorado, USA: National Center for Atmospheric Research), 113.

Smagorinsky, J. (1963). General circulation experiments with the primitive equations: I. The basic experiment. *Mon. Weather Rev.* 91, 99–164. doi: 10.1175/1520-0493(1963)091<0099:GCEWTP>2.3.CO;2

Smith, R. W., Bianchi, T. S., Allison, M., Savage, C., and Galy, V. (2015). High rates of organic carbon burial in fjord sediments globally. *Nat. Geosci.* 8, 450–453. doi: 10.1038/ngeo2421

Soto-Riquelme, C., Pinilla, E., and Ross, L. (2023). Wind influence on residual circulation in patagonian channels and fjords. *Continental Shelf Res.* 254, 104905. doi: 10.1016/j.csr.2022.104905

Stigebrandt, A. (1990). On the response of the horizontal mean vertical density distribution in a fjord to lowfrequency density fluctuations in the coastal water. *Tellus A: Dynamic Meteorology Oceanography* 42, 605–614. doi: 10.3402/tellusa.v42i5.11902

Stigebrandt, A. (2012). "Hydrodynamics and Circulation of Fjords," in *Encyclopedia of Lakes and Reservoirs*. Eds. L. Bengtsson, R. W. Herschy and R. W. Fairbridge (Springer Netherlands, Dordrecht), 327–344. doi: 10.1007/978-1-4020-4410-6247

Valle-Levinson, A. (2010). *Contemporary Issues in Estuarine Physics* (Cambridge University Press). doi: 10.1017/CBO9780511676567

Valle-Levinson, A., Caceres, M. A., and Pizarro, O. (2014). Variations of tidally driven three-layer residual circulation in fjords. *Ocean Dynamics* 64, 459–469. doi: 10.1007/s10236-014-0694-9

Valle-Levinson, A., Sarkar, N., Sanay, R., Soto, D., and León, J. (2007). Spatial structure of hidrography and flow in a Chilean fjord. *Estuaries coasts* 30, 113–126. doi: 10.1007/BF02782972

Viddi, F. A., Hucke-Gaete, R., Torres-Florez, J. P., and Ribeiro, S. (2010). Spatial and seasonal variability in cetacean distribution in the fjords of northern patagonia, Chile. *ICES J. Mar. Sci.* 67, 959–970. doi: 10.1093/icesjms/fsp288

Wan, D., Hannah, C. G., Cummins, P. F., Foreman, M. G. G., and Dosso, S. E. (2022). Wind-driven currents in a "wide" narrow channel, with application to douglas channel, bc. *J. Geophysical Research: Oceans* 127, e2021JC017887. doi: 10.1029/2021JC017887

Winant, C. D. (2008). Three-dimensional residual tidal circulation in an elongated, rotating basin. *J. Phys. Oceanography* 38, 1278–1295. doi: 10.1175/2007JPO3819.1